Version of Record: https://www.sciencedirect.com/science/article/pii/S1618866719306508
Manuscript_1806257b510cbe2bd59d6c0b2bd7f27b

Street tree health from space? An evaluation using WorldView-3 data and the Washington D.C. Street Tree Spatial Database

Fang Fang[a,b], Brenden McNeil[a], Timothy Warner[a], Gregory Dahle[c], Earl Eutsler[d]

[a] Department of Geology and Geography, West Virginia University, Morgantown, WV, 26505, USA

[b]Department of Urban and Regional Planning, University of Illinois at Urbana-Champaign, Champaign, Illinois, 61820, USA

[c] Division of Forestry & Natural Resources, West Virginia University, Morgantown, WV, 26505, USA

[d]Urban Forestry Division, District Department of Transportation, Washington, DC, 20003, USA

© 2020 published by Elsevier. This manuscript is made available under the Elsevier user license
https://www.elsevier.com/open-access/userlicense/1.0/

Street tree health from space? An evaluation using WorldView-3 data and the Washington D.C. Street Tree Spatial Database

Abstract

Spatially accurate and timely information on tree health is an essential component of maintaining sustainability in a species-rich urban setting. Our objective was to evaluate the potential of WorldView-3 (WV-3) satellite images from June 11th, July 30th and August 30th, 2017 to detect field-measured health condition classes of 2308 trees within the District of Columbia Department of Transportation's Street Tree Spatial Database. For each street tree in each image, we measured six vegetation indices (VIs), and find that NDVI1 (defined as the normalized ratio of the red and the first of the near infrared bands) on the July image shows the strongest statistical difference among the VI values of trees classified in the field during 2017 as in good, fair, or poor health condition. This result confirms that high spatial resolution remote sensing images provided the opportunity for a timely tree health assessment at individual tree crown level. Notably, the variability in VI attributable to health condition classes is smaller than the large declines in VIs between the June and August image dates. This greendown phenological pattern occurs similarly for trees in all health condition classes, and is thus an essential consideration when comparing VIs from different years or months for tree health assessment. The tree health condition discrimination was overwhelmed by this greendown phenology and the spectral variability in these species-rich urban settings. Based on these findings, we propose useful strategies of using these high-resolution WV-3 data for street tree health management in other cities.

1. Introduction

More than half of the world's population now lives in cities (Lederbogen et al., 2011) and tree health conditions have been widely recognized as central for the sustainability of these expanding urban populations (Huang et al., 2007; Xiao and McPherson 2005). As a case study representative of other large urban centers worldwide (Gregg, Jones and Dawson 2003; McPherson et al., 1994; Nowak and Crane, 2002; Wong and Yu, 2005), our study focuses on Washington D.C., where nearly 30% of the land surface is covered by urban trees. Each year, these trees provide D.C. with $3.6 billion in structural values (e.g. providing shade to cool buildings), and $2.5 million in functional values like pollution removal (Nowak et al., 2006). There are approximately 1,928,000 trees (Nowak et al., 2006) within the D.C. boundaries, and extensive efforts with an annual budget around $15.5 million are directed toward urban tree management (e.g. planting, pruning, removing, maintaining). To improve this urban tree management process, District Department of Transportation (DDOT) has created a Street Tree Spatial Database to track the location and attributes (e.g. DBH, health condition class, and species) of all street trees since 2006, and they have expended considerable effort to regularly update this database.

Poor tree health can be caused by biotic agents like fungi, bacteria or viruses, or abiotic agents such as drought or freezing injury (Jackson, 1986). In addition, because of urban environmental disturbances such as air pollution, compacted soil, damage from traffic or pedestrians, and improper planting, urban street trees typically face a more stressful environment compared with trees in native forests (McIntyre, 2000). Previously, one of the most common trees in D.C., the American elm (*Ulmus americana*), was almost entirely lost to Dutch elm disease (*Ophiostoma spp.*, Banfield, 1968; Nowak et al., 2006). Currently, over 30% of the tree population in D.C. is at risk of being lost to the Asian Longhorned Beetle (*Anoplophora glabripennis*, Nowak et al., 2006). Less severe, more chronic agents, such as Bacterial leaf scorch (Harris and Balci, 2015) also affect street trees in D.C. These diseases and pests are often

53 the initiators of diminished tree health, which can directly lead to tree death, ensuing economic
54 losses, and deteriorating quality of life in urban settings (Harris and Balci, 2015; Nowak et al.,
55 2006).

56 Tree health is traditionally monitored via field surveys. However, there is great potential for
57 using remote sensing to monitor tree health (Ward and Johnson, 2007). Poor health is often
58 expressed by lowered leaf water or chlorophyll content, which both affect the spectral reflectance
59 of trees (Asmaryan et al., 2013; Chaves et al., 2002; Eitel et al., 2011; Huang et al., 2007;
60 Knipling, 1970; Xiao and McPherson, 2005; Sankaran et al., 2010). Indeed, promising research
61 from non-urban forests has demonstrated potential for evaluating vegetation health from
62 multispectral and hyperspectral data (Delalieux et al., 2009; Eitel et al., 2011; Franke and Menz,
63 2007; Lambert et al., 2013; Huang et al., 2007; Michez et al., 2016; Nasi et al., 2018; Senf, Seidl
64 and Hostert 2017; Xiao and McPherson, 2005). For instance, increased presence of
65 Huanglongbing disease (*Candidatus* Liberibacter spp.) was associated with decreased NIR
66 reflectance in citrus trees (Li et al., 2012). Given the sensitivity of the NIR spectral region to tree
67 health, various vegetation indices like the normalized difference vegetation index (NDVI) are
68 often correlated with poor health (Eitel et al., 2011; Xiao and McPherson, 2005). Nasi et al (2018)
69 claimed that UAV images produced better results identifying bark beetle infestation at individual
70 crown level for Norway spruce due to their finer spatial resolution. Yet, despite the well-
71 established linkages among spectral reflectance and tree health at pixel and leaf scales in rural
72 settings, there remain substantial challenges for researchers and managers wishing to apply
73 satellite data to assess the health of street trees at the biologically-meaningful, and necessary
74 management in the species-rich urban settings at individual tree crowns.

75 Here, we take advantage of promising new field and image datasets to evaluate the current
76 prospects for meeting these challenges by matching 2308 street trees in the DDOT Street Tree
77 Spatial Database with atmospherically corrected WorldView-3 spectral data collected on June
78 11th, July 30th, and August 30th, 2017. Recently, an exploratory analysis of trees in various cities

around the world found that the high spatial, radiometric, and spectral resolution of WV-3 data was useful for resolving individual urban trees, and for tracking spectral changes consistent with declining tree health (Au, 2018). Building from that work, the goal of our study is to systematically evaluate whether WV-3 data can be used to detect a statistical difference and further discriminate street tree health marked by the DDOT as having different field-assessed condition classes (e.g. good, fair, poor).

We explicitly examine essential remote sensing data considerations in the areas of useful spectral regions and temporal variability in order to support the decision-making process for urban forest management. First, to take full advantage of the high spatial resolution of WV-3 data, we present a two-step process to identify tree crown pixels at individual tree crown level on the field and image data. Second, since tree health may affect the visible, red edge, and NIR portions of the spectrum, we evaluate which spectral vegetation indices (VIs) might best describe the spectral differences in street tree health. Finally, we consider how non-health related spectral variability within the growing season (e.g. related to such factors such as greendown phenology, Elmore et al., 2012; Reaves et al., 2018) may affect prospects for street tree health assessments. Based on our findings, we discuss two promising strategies for using high-resolution satellite data in street tree health management.

2. Methods

2.1 Study area

Washington D.C. has extensive urban forests covering much of the city (Andrada II et al., 2015). Besides trees under private ownership or various local agencies (e.g. National Capital Planning commission, District of Columbia's Department of Parks and Recreation), the Urban Forestry Administration (UFA) is the District's governmental agency responsible for planting, pruning, removal and other routine maintenance of the remaining street trees in the public spaces. These street trees comprise approximately 9% of the entire Washington D.C. urban forest

(Government of the District of Columbia, 2010). In order to maximize the overlap of this street tree database with available cloud-free archived WV-3 imagery, we set our study site within Washington D.C. to a 25 km^2 area (**Figure 1**).

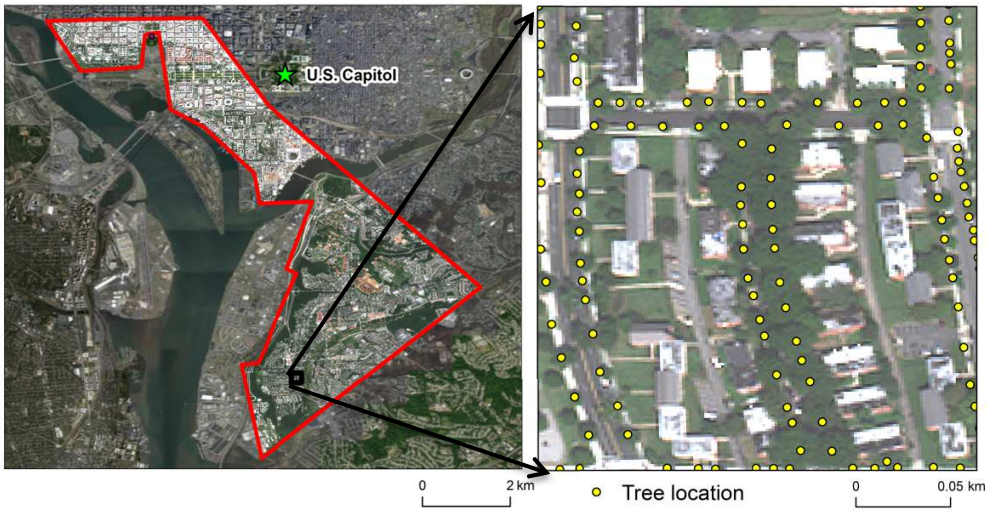

Figure 1. a) Study area (within red boundary) in the District of Columbia. b) Portion of the digitized street tree locations superimposed on a WorldView-3 true color image from August 30, 2017

2.2 Image datasets

We purchased 12 sets of WV-3 cloud-free Atmospheric Compensation (ACOMP) imagery from a DigitalGlobe vendor (**Supplemental Table s1**). The ACOMP products mitigate the effects of haze and atmospheric scattering and provide normalized surface reflectance values (reflectance index) of the surface objects for both panchromatic and multi-spectral images (DigitalGlobe, Inc. 2016). The ACOMP products also include radiometric corrections (e.g. non-response detector filling, calibrations of the relative radiometric response between detectors), as well as sensor correction rectification with respect to the internal detector geometry and scan distortion (Ferreira et al., 2019). To independently validate the ACOMP product, we used 50 pixels from pseudo-invariant objects distributed throughout the study area to confirm that there is no significant

difference (Supplemental **Table s2**) in the mean NDVI on different dates (Hadjimitsis et al., 2009).

The data contain eight multispectral bands (B_1 … B_8) at a spatial resolution of 1.2 m and one panchromatic band at a spatial resolution of 0.3m: Panchromatic band (450 – 800 nm), Coastal (B_1: 400 – 450 nm), Blue (B_2: 450 – 510 nm), Green (B_3: 510 – 580 nm), Yellow (B_4: 585 – 625 nm), Red (B_5: 630 – 690 nm), Red edge (B_6: 705 – 745 nm), NIR-1 (B_7: 770 – 895 nm) and NIR-2 (B_8: 860 – 1040 nm). In order to evaluate the ability of imagery to assess tree health at different points during the leaf-on period, we selected three archived WV-3 images from June 11, 2017 (Day of year (DOY) 162), July 30, 2017 (DOY 211), and August 30, 2017 (DOY 242). The off nadir view angles of these images were 22.2°, 14.0 ° and 14.7° respectively. We used cubic convolution resampling to individually register each image to the DDOT LiDAR Reflective surface (District of Columbia Government, 2009) (RMSE < 1 pixel).

2.3 Field dataset

We downloaded the tree inventory data from the DDOT Street Spatial Database on March 8th 2018 (District of Columbia Government, 2018). This D.C. tree inventory was first created by Casey Trees Foundation in 2002 and has been updated by the Urban Forestry Administration since 2006. The dataset contains attributes of all street trees such as the tree stem coordinates, species common name, tree health condition class, and diameter at breast height (DBH). In total, there are 18,434 tree stems within our 25km^2 study area. As shown in **Figure 1**, tree locations are digitized as yellow dots based on the field measurements, which also include a few invalid tree locations due to the inconsistency of the dates between field measurement and image acquisition. Even with the high spatial resolution of WV-3, most trees were too small to provide enough spectral data, so we restricted our study to mature trees with DBH greater than 10.16 cm (4 inches) (Memiaghe et al., 2016; Nascimebene et al., 2009). The database describes five classes of tree health condition: excellent, good, fair, poor and dead. A given tree health

condition is determined in the field by the quality of a crown and growth vigor (**Table 1&2**). Only 30 trees were marked excellent, so we merged these trees with those marked "good". Furthermore, we did not include trees classified as "dead", or trees that did not contain at least 3 pixels that met our NDVI-based tree delineation criteria (see section 2.4). Our final dataset included 1854 trees in the good health condition class, 388 in the fair health condition class, and 66 trees in the poor health condition class, for a total sample size of 2380 trees. Even though there are 95 tree species in this sample, just under half of the trees are from five tree species: willow oak (*Quercus phellos*), red maple (*Acer rubrum*), pin oak (*Quercus palustris*), American elm (*Ulmus americana*), and red oak (*Quercus rubra*).

Table 1 Field tree health condition assessment parameters

Parameter	Crown Quality Score	Vigor Score
0	0	0
<25%	1	1
25-50%	2	2
50-75%	3	3
75-100%	4	4
Notes	Percentage of crown that is free from dieback, disease, and/or other physiological abnormality	Year-over-year shoot elongation and distribution of growth throughout crown.

Table 2 Field tree health condition scores

Condition	Score
Excellent	≥7
Good	5 to 6
Fair	3 to 5
Poor	2 to 3
Dead	0 to 1

2.4 Extracting pixels for tree crowns

We used a two-step conservative approach to extract pixels belonging to the crown of an individual tree. First, we extracted all pixels within a radial buffer from the spatial coordinates of each tree trunk. To avoid introducing uncertainties from allometric equations from the 95 different tree species in our study area, we used the average DBH (34.8 cm) and a single allometric equation (Gering and May, 1995) to determine an average crown diameter of 9.1 m. Accordingly, we applied a buffer radius of 4.55 m as the first step in identifying each tree crown area. Second, in order to avoid the confounding influence of background, invalid tree locations and non-vegetated pixels (e.g. pavement), we masked any pixels with NDVI1 values less than 0.5 (**Figure 2**, Li et al., 2015; Karlson et al., 2016). Using a random subset of 100 tree-crown objects, we visually confirmed from pan-sharpened imagery that this two-step tree procedure was effective in extracting pixels within each individual tree crown. We note that for large trees, the extracted pixels conservatively include only the central portion of the tree crown.

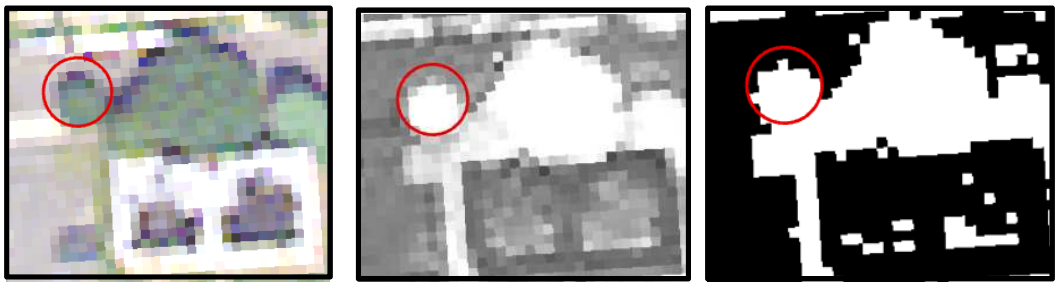

a b c

Figure 2. Example of the two-step of extracting pixels from tree crown-area. Red circle: 4.55m radial tree crown buffer. a) True Color WV-3 image from August 30, 2017. b) NDVI1 calculated from the NIR1 and red bands. c) Application of the 0.5 NDVI1 threshold, showing the defined tree crown-object as all the white pixels whose majority area falls within the red radial crown buffer.

The tree crown-objects in our study are generally not affected by variable spectral reflectance of the background, because we are only examining public street trees, and not urban trees in park-like settings with backgrounds dominated by other vegetation (e.g. grass). Our field observations and visual examination of available leaf-off imagery revealed that the street trees have two distinct types of backgrounds: 1) a relatively pure background of pavement (often with a metal

187 grate surrounding the trunk), and 2) a mixed background consisting of pavement and a tree box
188 containing soil, bark mulch, and ground vegetation. Yet, even for the 66 trees within the poor
189 health class where thinning leaf area might cause the background to have a consequential effect
190 on the spectral reflectance of a tree crown-object (49 trees with mixed background and 17 trees
191 with pure background of pavement), we found no statistical difference in NDVI of trees sorted by
192 these two background types (**Supplemental Table s3**).

193 **2.5 Data analysis**

194 We focus on VIs because they describe expected changes to multiple parts of the spectral
195 profiles from trees with different tree health conditions. Our assumption is that the shape of the
196 spectrum is a generally more sensitive indicator of tree health than the magnitude of the
197 reflectance in any one band. This was supported by preliminary work, in which we examined
198 other image spectral information, including raw reflectance on each multi-spectral band, and
199 panchromatic (30 cm pixel resolution) image texture within the crown objects. This preliminary
200 work indicated that VIs are useful and straightforward means to statistically test the difference
201 between tree health classes.

202 Based on knowledge of how tree health might affect spectral reflectance in the NIR, green,
203 red, and yellow portions of the spectrum, we calculated six vegetation indices from each of the
204 three sets of images. NDVI1 using the red and first NIR band, NDVI2 using red and the second
205 NIR band, Red Edge NDVI (REDNVI), Green yellow ratio (GY), and the Green Red ratio (GR)
206 (Boochs et al., 1990; Fang et al., 2018; Karlson et al., 2016; Pontius et al., 2008). After we
207 extracted and averaged the pixel VI values from each tree, we tested for statistical differences
208 among the VI values of trees in different health condition classes, and repeated these tests for
209 each combination of VI and image date. Because at least one of the assumptions of ANOVA (e.g.
210 normally distributed residuals, or equal variances) were violated for each VI/Image combination,
211 we used the non-parametric Wilcoxon/Kruskal-Wallis test to identify significant differences of

distributions for VI values within each health class. The non-parametric Wilcoxon/Kruskal-Wallis test has the null hypothesis that the medians are same between different classes, and it is resistant to outliers. Chi-square value is calculated to test this null hypothesis. We identified the most sensitive VI/image date combination as the one that achieved the highest Chi-square value. We also used other archived ACOMP WV-3 imagery to track the most sensitive VI/image under different health condition classes from 2014 to 2017.

After the statistical analysis, we applied Random Forest machine learning algorithms to directly discriminate tree health classes from VIs, raw reflectance on each multispectral band, and panchromatic (30cm pixel resolution) image texture metrics extracted from each crown object. We used ¾ of the data as training and ¼ as validation. The performance of prediction will be affected by class imbalance, and under-prediction will occur especially for less abundant classes due to their true proportion to the training dataset. In our dataset, we have 1854 trees in the good health condition class, 388 in the fair health condition class, but only 66 trees in the poor health condition class. Therefore, we applied the up-sampling method for each of training set prior to this Random Forest classification in order to avoid bias induced by class imbalance between three types of health conditions (Maxwell, Warner and Fang 2018). After applying the up-sampling method we got equally distributed classes. Last, we recorded kappa to evaluate the performance for tree health condition classification process.

3 Results

Within each of the three image dates, the VI values of trees in good, fair and poor health condition classes are all highly statistically different (**Table 3**), and tree health condition classes had the expected effects on VIs. Trees in the poor health condition class had the lowest mean VI values, trees in the fair health condition class had intermediate mean VI values, and trees in the good health condition class had the highest mean VI values (**Figure 3**). As measured by the highest Chi-square from the Wilcoxon/Kruskal-Wallis analyses, the most sensitive VI was NDVI on the July 30th (DOY 211) image **(Table 3, Supplemental figure s1).**

It also has a statistically significant difference between the top five tree species (**Figure 4**). The VIs that included red edge bands were the next most sensitive, followed by the VIs using only visible light bands. For tree health condition discrimination using Random Forest, the kappa is 2.53% to classify three classes.

Table 3 Chi-square values from non-parametric Wilcoxon/Kruskal-Wallis tests of statistical difference in VI values among trees in good, fair and poor health condition classes. All tests were significant at $p < 0.001$. The bold value denotes the most sensitive image date/VI combination.

Vegetation Index	June	July	August
NDVI1	65.97	**102.46**	77.80
NDVI2	70.89	94.18	75.57
RENDVI1	73.71	83.78	46.12
RENDVI2	72.17	72.17	41.16
Green Yellow ratio	37.74	48.96	23.61
Green Red ratio	46.43	48.79	25.14

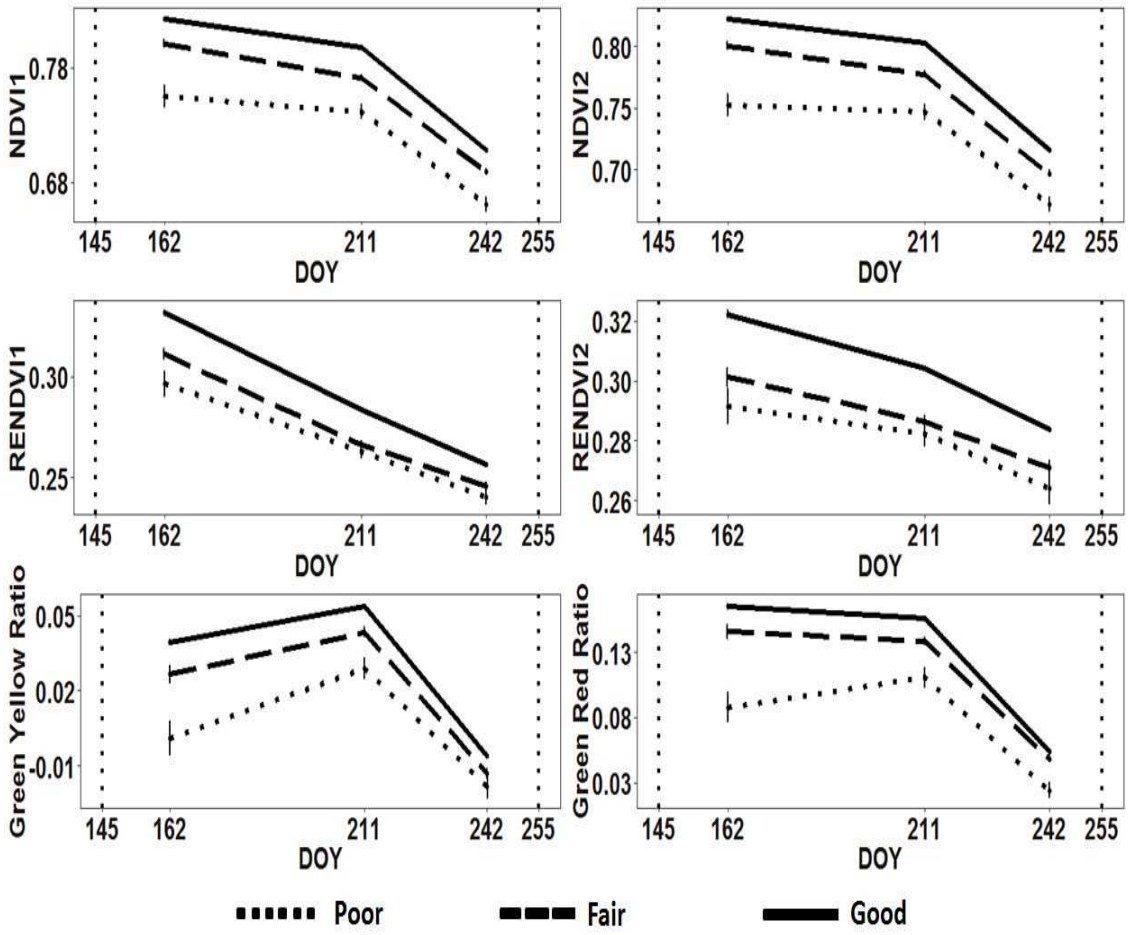

Figure 3 Mean (error bars represent +/- 1 standard error) vegetation index values for trees in three health condition classes. Based on webcam and Landsat phenology data for our study area (from Figure 7 in Elmore et al. 2012), we also show vertical dotted lines to mark the average DOY of full leaf expansion (DOY145), and leaf senescence (DOY 255).

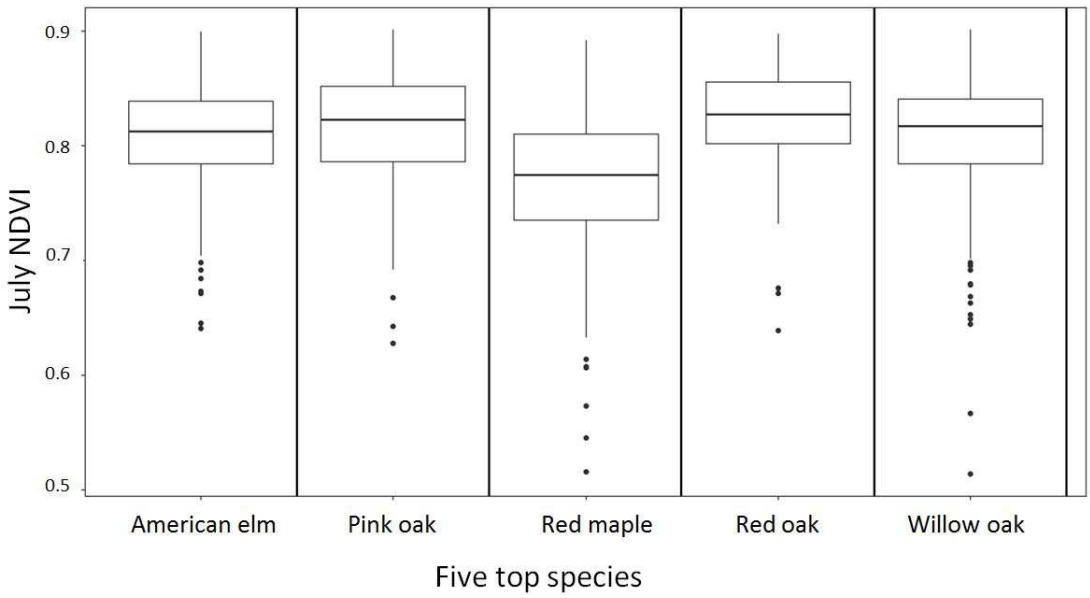

Figure 4. Significant ($p<0.0001$) tree species differences in NDVI1 on the July 30th, 2017 image.

4 Discussion

4.1 Statistical comparison of VIs for tree health condition assessment

We find that the most sensitive VI for detecting tree health condition classes was NDVI1. Previous studies illustrated the usefulness of red edge NDVI for early observation of trees with poor health conditions (Eitel et al., 2011; Karlson et al., 2016), but we find that the traditional NDVI outperformed red edge NDVI in testing the statistical difference of trees in poor, fair and good condition classes (**Table 3**). Within the DDOT field surveys, tree health condition classes are evaluated based on the crown quality and vigor (**Table 1 & 2**). Our results suggest that NDVI1 best matches with these field-observed health symptoms. Field observers also note changes in leaf color when assigning a tree health condition class, with the increased presence of yellow leaves leading to a fair or poor health assessment. By showing that the Green Yellow ratio (calculated from visible bands) is significantly different between tree health condition classes, our study reconfirms the potential utility of yellow band (Karlson et al., 2016) to

describe tree health condition classes. Yet, NDVI1 outperformed Green Yellow ratio, which suggests that the change in NIR band reflectance for trees under poor health class is greater than the change in yellow band. This is likely because field-based tree health evaluators more strongly associate health with a change of leaf area rather than a change in leaf color.

We also focused on the most sensitive index, NDVI1, to evaluate how NDVI1 varied by tree species. Among the five most abundant tree species that had a large enough sample size to statistically analyze, we find that there are significant differences in NDVI1 (**Figure 4**). Red maple had the lowest NDVI1, while red oak had the highest. Based on this finding of variability in VI among species, we also tried to repeat our analysis of the most sensitive VI on a species-specific basis. However, for each species, this analysis was hampered by low sample sizes in different health condition classes (**Supplemental Table s4**). Nevertheless, this exploratory species-specific analysis suggests that the most sensitive VI may not be consistent across different tree species (**Supplemental Table s5-9**). Thus, even while we find NDVI1 to be the best all-purpose VI for showing the statistical difference with expected direction between tree health condition classes, individual species may exhibit tree health condition symptoms that better align with spectral variability described by other VIs.

4.2 Effects of image acquisition date and greendown phenology

According to an analysis by Elmore et al. (2012) of the Landsat data record and phenology web camera (phenocam) imagery, the leaf-on period in Washington D.C extends from a full leaf expansion date around DOY 145 to an average date of leaf senescence around DOY 255 (**Figure 3**). These Landsat and phenocam data from our study area also both evidence a steady decline in greenness during this leaf-on period (Elmore et al., 2012). Importantly, our analysis from the three images illustrates that the ACOMP WV-3 data also captures this greendown phenology (**Figure 3**). As we detail in section 4.3, this decline in greenness, or greendown (Reaves et al., 2018), during the leaf-on period is a pervasive feature

296 in vegetation phenology, and has important implications for selecting high resolution satellite
297 data to assess street tree health.

298 We found that the July image (DOY 211), midway through the leaf-on period, appears to
299 be the strongest for describing the statistical difference in NDVI1 based on field-measured tree
300 health condition classes **(Table 3).** We suggest that the June image (DOY 162) is less helpful
301 describing tree health condition symptoms because this date is close to the full leaf expansion
302 date for some tree species. This timing could cause some trees to have the spectral effects of
303 tree health convolved with spectral effects of a late full leaf expansion date. Indeed, in our
304 exploratory species-specific analyses, we found that for red maple, and American elm, the VIs
305 from the June image were actually more sensitive than from the July image (**Supplemental**
306 **Tables s5-s7**). We suggest that the weaker strength of the June image may be driven by
307 relatively late leaf out dates of other species, including the two most common species, Willow
308 oak and pin oak. In these two oak species, the July image was more sensitive in detecting a
309 statistical difference between tree health classes (**Supplemental Tables s8 & s9)**. For all
310 species, the August image (DOY 242) may have been too close to the average leaf senescence
311 date, which could cause some trees to have the spectral effects of tree health convolved with
312 spectral effects of leaf senescence. Thus, we recommend using image dates that are safely
313 within the middle of the leaf-on period.

314 A further supplemental analysis revealed that our study greatly benefitted from the
315 availability of field-measured heath condition data collected at the same time as the imagery
316 during the 2017 growing season. We used other archived ACOMP WV-3 imagery from 2014,
317 2015, and 2016 to track the NDVI1 of all the trees in different 2017 health condition classes
318 (**Table 1 & 2**). This analysis shows that there was limited statistical difference in NDVI1
319 among trees in different health classes in the years preceding the field-based health assessment
320 in 2017 (Supplemental **Figure s2**).

4.3 Strategies for using remote sensing data for street tree health assessment and management

We applied Random Forest machine learning algorithms to directly discriminate tree health classes at individual tree crown level. However, the kappa coefficient from this analysis was extremely weak (2.53%), which reveals that the ability to directly discriminate tree health classes is overwhelmed by greendown phenology and other drivers of spectral reflectance in this complex urban environment (**Supplemental Table s10**). Nevertheless, our findings evidencing a robust, statistical difference in NDVI1 among the health classes of individual street trees does highlight useful approaches for advancing the integration of high-resolution multispectral satellite data into street tree health research and management in the future. We recommend using WV-3 images to assess tree health at individual crown level in other cities. First, we recommend using an image from midway through the leaf-on period to minimize VI change related to tree phenology, and especially change associated with leaf expansion, greendown, and leaf senescence. Researchers could use a VI on a single-date image during this leaf-on period to identify priority trees for field-based street tree health evaluation. Second, we recommend applying our approach to regions with similar species components as Washington D.C.

We also suggest other productive lines of future research that can potentially overcome remaining challenges to remotely assessing the health of individual trees. First, researchers and street tree managers could use multi-year, anniversary-date imagery to track VIs of individual trees over time. Furthermore, researchers or managers wishing to target health assessments to individual tree species may find it advantageous to match the anniversary date and the selected diagnostic VI to the most sensitive date/VI for the target species. Future studies may profit from directly assessing these health-related crown structural changes instead of spectral change

using high-resolution LiDAR (Plowright et al., 2016), and using terrestrial and UAV platforms (Dash et al. 2018; Disney, 2018).

5 Conclusion

We evaluate the ability of six WV-3 VIs extracted from tree street tree crown-objects on images from three different dates to detect differences among the field-measured health condition classes of 2308 street trees in central Washington D.C. We find that spectral data are statistically useful for tree health analysis, which can be effectively extracted from imagery by using an NDVI-threshold mask within a buffer around a field-measured GPS point of the tree trunk. Extracted VIs from all image dates revealed highly significant differences among tree health condition classes in expected direction. Moreover, NDVI1 from an image from the middle of the leaf-on period has the most potential to assess the health condition classes of street trees in central Washington D.C.

As the availability of high spatial resolution remote sensing images increases, there will be increasing demands and interests to monitor tree health conditions via remote sensing, and to augment forest datasets or inventory in urban settings. Our results provide insight into the utility of high-resolution satellite data as a tool providing timely and extensive information for research and tree health management in urban environment. Our case study thus provides the basis for monitoring and discriminating tree health from space, which will further improve urban forest planning strategies in order to maintain the social, economic and environmental benefits of urban trees.

References

Andrada II, R., Deng, J., Gazal, K., 2015. Exploring people ' s preferences on specific attributes of urban forests in Washington DC : A conjoint approach 7, 200–209. https://doi.org/10.5897/JHF2015.

Asmaryan, S., Warner, T.A., Muradyan, V., Nersisyan, G., 2013. Mapping tree stress associated with urban pollution using the WorldView-2 Red Edge band. Remote Sens. Lett. https://doi.org/10.1080/2150704X.2012.715771

Au, 2018. An integrated approach to tree stress monitoring. Arborist news. http://geocarto.com.hk/readings/aug2018_issue/#page/1 (accessed 20 September 2018)

Banfield, W.M., 1968. Dutch Elm Disease Recurrence and Recovery in American Elm. J. Phytopathol. https://doi.org/10.1111/j.1439-0434.1968.tb02345.x

Boochs, F., Kupfer, G., Dockter, K., Kuhbaüch, W., 1990. Shape of the red edge as vitality indicator for plants. Int. J. Remote Sens. https://doi.org/10.1080/01431169008955127

Chaves, M.M., Pereira, J.S., Maroco, J., Rodrigues, M.L., Ricardo, C.P.P., Osório, M.L., Carvalho, I., Faria, T., Pinheiro, C., 2002. How plants cope with water stress in the field. Photosynthesis and growth. Ann. Bot. https://doi.org/10.1093/aob/mcf105

Dash, J., Pearse, G., & Watt, M. (2018). UAV multispectral imagery can complement satellite data for monitoring forest health. *Remote Sensing*, 10(8), 1216.

Delalieux, S., Somers, B., Verstraeten, W.W., van Aardt, J.A.N., Keulemans, W., Coppin, P., 2009. Hyperspectral indices to diagnose leaf biotic stress of apple plants, considering leaf phenology. Int. J. Remote Sens. https://doi.org/10.1080/01431160802541556

District of Columbia Government. (2009). LiDAR - Reflective Surface. Retrieved from https://dcgis.maps.arcgis.com/home/item.html?id=1057f1898171442487816b7f891dc2fc

District of Columbia Government. (2018). Urban Forestry Street Trees. Retrieved from http://opendata.dc.gov/datasets/f6c3c04113944f23a7993f2e603abaf2_23

DigitalGlobe Inc. 2016. Digitalglobe Atmospheric Compensation, https://explore.digitalglobe.com/AComp.html (accessed 8 March 2018)

Disney, M. (2018). Terrestrial Li DAR: a three-dimensional revolution in how we look at trees. *New Phytologist*.

Eitel, J.U.H., Vierling, L.A., Litvak, M.E., Long, D.S., Schulthess, U., Ager, A.A., Krofcheck, D.J., Stoscheck, L., 2011. Broadband, red-edge information from satellites improves early stress detection in a New Mexico conifer woodland. Remote Sens. Environ. https://doi.org/10.1016/j.rse.2011.09.002

Elmore, A.J., Guinn, S.M., Minsley, B.J., Richardson, A.D., 2012. Landscape controls on the timing of spring, autumn, and growing season length in mid-Atlantic forests. Glob. Chang. Biol. https://doi.org/10.1111/j.1365-2486.2011.02521.x

401 Fang, F., McNeil, B.E., Warner, T.A., Maxwell, A.E., 2018. Combining high spatial resolution
402 multi-temporal satellite data with leaf-on LiDAR to enhance tree species discrimination at
403 the crown level. Int. J. Remote Sens. https://doi.org/10.1080/01431161.2018.1504343

404 Ferreira, M. P., Wagner, F. H., Aragão, L. E., Shimabukuro, Y. E., & de Souza Filho, C. R. (2019).
405 Tree species classification in tropical forests using visible to shortwave infrared WorldView-
406 3 images and texture analysis. ISPRS Journal of Photogrammetry and Remote Sensing, 149,
407 119-131.

408 Franke, J., Menz, G., 2007. Multi-temporal wheat disease detection by multi-spectral remote
409 sensing. Precis. Agric. https://doi.org/10.1007/s11119-007-9036-y

410 Gering, L.R., May, D.M., 1995. The relationship of diameter at breast height and crown diameter
411 for four species groups in Hardin County, Tennessee. South. J. Appl. Forestry, 19(4), 177–
412 181.

413 Government of the District of Columbia/ District Department of Transportation. (2010). *District
414 of Columbia Assessment of Urban Forest Resources and Strategy*. Washington D.C
415 https://ddot.dc.gov/sites/default/files/dc/sites/ddot/publication/attachments/dc_assessm
416 ent_urban_forest_resources_strategy_2010-06.pdf (accessed 8 October 2018)

417 Gregg, J.W., Jones, C.G., Dawson, T.E., 2003. Urbanization effects on tree growth in the vicinity
418 of New York City. Nature. https://doi.org/10.1038/nature01728

419 Hadjimitsis, D. G., Clayton, C. R. I., & Retalis, A. (2009). The use of selected pseudo-invariant
420 targets for the application of atmospheric correction in multi-temporal studies using
421 satellite remotely sensed imagery. International Journal of Applied Earth Observation and
422 Geoinformation, 11(3), 192-200.

423 Harris, J.L., Balci, Y., 2015. Population structure of the bacterial pathogen Xylella fastidiosa
424 among street trees in Washington D.C. PLoS One.
425 https://doi.org/10.1371/journal.pone.0121297

426 Huang, W., Lamb, D.W., Niu, Z., Zhang, Y., Liu, L., Wang, J., 2007. Identification of yellow rust in
427 wheat using in-situ spectral reflectance measurements and airborne hyperspectral imaging.
428 Precis. Agric. https://doi.org/10.1007/s11119-007-9038-9

429 Jackson, R.D., 1986. Remote Sensing of Biotic and Abiotic Plant Stress. Annu. Rev. Phytopathol.
430 https://doi.org/10.1146/annurev.py.24.090186.001405

431 Karlson, M., Ostwald, M., Reese, H., Bazié, H.R., Tankoano, B., 2016. Assessing the potential of
432 multi-seasonal WorldView-2 imagery for mapping West African agroforestry tree species.
433 Int. J. Appl. Earth Obs. Geoinf. https://doi.org/10.1016/j.jag.2016.03.004

434 Knipling, E.B., 1970. Physical and physiological basis for the reflectance of visible and near-
435 infrared radiation from vegetation. Remote Sens. Environ. https://doi.org/10.1016/S0034-
436 4257(70)80021-9

437 Lambert, J., Drenou, C., Denux, J.P., Balent, G., Cheret, V., 2013. Monitoring forest decline
438 through remote sensing time series analysis. GIScience Remote Sens.
439 https://doi.org/10.1080/15481603.2013.820070

Lederbogen, F., Kirsch, P., Haddad, L., Streit, F., Tost, H., Schuch, P., Wüst, S., Pruessner, J.C., Rietschel, M., Deuschle, M., Meyer-Lindenberg, A., 2011. City living and urban upbringing affect neural social stress processing in humans. Nature. https://doi.org/10.1038/nature10190

Li, D., Ke, Y., Gong, H., Li, X., 2015. Object-based urban tree species classification using bi-temporal worldview-2 and worldview-3 images. Remote Sens. https://doi.org/10.3390/rs71215861

Li, X., Lee, W.S., Li, M., Ehsani, R., Mishra, A.R., Yang, C., Mangan, R.L., 2012. Spectral difference analysis and airborne imaging classification for citrus greening infected trees. Comput. Electron. Agric. https://doi.org/10.1016/j.compag.2012.01.010

Maxwell, A. E., Warner, T. A., & Fang, F. (2018). Implementation of machine-learning classification in remote sensing: An applied review. International Journal of Remote Sensing, 39(9), 2784-2817.

McIntyre, N.E., 2000. Ecology of Urban Arthropods: A Review and a Call to Action. Ann. Entomol. Soc. Am. https://doi.org/10.1603/0013-8746(2000)093[0825:EOUAAR]2.0.CO;2

McPherson, G.E., Nowak, D.J., Rowntree, R.A., Mcpherson, E.G., Nowak, D.J., Rowntree, R.A., 1994. Chicago's urban forest ecosystem: Results of the Chicago Urban Forest Climate Project, General Technical Report. https://doi.org/10.1111/pace.12264

Memiaghe, H.R., Lutz, J.A., Korte, L., Alonso, A., Kenfack, D., 2016. Ecological Importance of Small-Diameter Trees to the Structure, Diversity and Biomass of a Tropical Evergreen Forest at Rabi, Gabon. PLoS One. https://doi.org/10.1371/journal.pone.0154988

Michez, A., Piégay, H., Lisein, J., Claessens, H., Lejeune, P., 2016. Classification of riparian forest species and health condition using multi-temporal and hyperspatial imagery from unmanned aerial system. Environ. Monit. Assess. https://doi.org/10.1007/s10661-015-4996-2

Nascimbene, J., Marini, L., Motta, R., Nimis, P.L., 2009. Influence of tree age, tree size and crown structure on lichen communities in mature Alpine spruce forests. Biodivers. Conserv. https://doi.org/10.1007/s10531-008-9537-7

Näsi, R., Honkavaara, E., Blomqvist, M., Lyytikäinen-Saarenmaa, P., Hakala, T., Viljanen, N., ... & Holopainen, M. (2018). Remote sensing of bark beetle damage in urban forests at individual tree level using a novel hyperspectral camera from UAV and aircraft. *Urban Forestry & Urban Greening*, *30*, 72-83.

Nowak, D., Hoehn, R., Crane, D., Stevens, J., Walton, J., 2006. Assessing Urban Forest Effects and Values: Washington, D.C.'s Urban Forest 24. https://doi.org/10.1525/bio.2011.61.1.10

Nowak, D.J., Crane, D.E., 2002. Carbon storage and sequestration by urban trees in the USA, in: Environmental Pollution. https://doi.org/10.1016/S0269-7491(01)00214-7

Plowright, A. A., Coops, N. C., Eskelson, B. N., Sheppard, S. R., & Aven, N. W. (2016). Assessing urban tree condition using airborne light detection and ranging. *Urban forestry & urban greening*, *19*, 140-150.

Pontius, J., Martin, M., Plourde, L., Hallett, R., 2008. Ash decline assessment in emerald ash borer-infested regions: A test of tree-level, hyperspectral technologies. Remote Sens. Environ. https://doi.org/10.1016/j.rse.2007.12.011

Reaves, V.C., Elmore, A.J., Nelson, D.M., McNeil, B.E., 2018. Drivers of spatial variability in greendown within an oak-hickory forest landscape. Remote Sens. Environ. https://doi.org/10.1016/j.rse.2018.03.027

Sankaran, S., Mishra, A., Ehsani, R., Davis, C., 2010. A review of advanced techniques for detecting plant diseases. Comput. Electron. Agric. https://doi.org/10.1016/j.compag.2010.02.007

Senf, C., Seidl, R., & Hostert, P. (2017). Remote sensing of forest insect disturbances: Current state and future directions. *International journal of applied earth observation and geoinformation*, *60*, 49-60.

Wong, N.H., Yu, C., 2005. Study of green areas and urban heat island in a tropical city. Habitat Int. https://doi.org/10.1016/j.habitatint.2004.04.008

Xiao, Q., McPherson, E.G., 2005. Tree health mapping with multispectral remote sensing data at UC Davis, California. Urban Ecosyst. https://doi.org/10.1007/s11252-005-4867-7

Ward, K. T., & Johnson, G. R. (2007). Geospatial methods provide timely and comprehensive urban forest information. *Urban Forestry & Urban Greening*, *6*(1), 15-22.

Supplemental

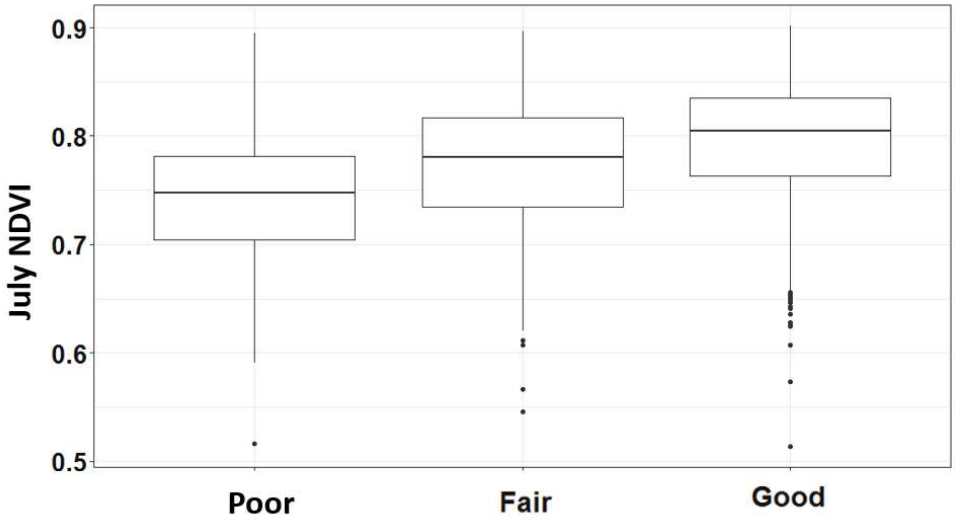

Figure s1 Boxplot for July NDVI between three types of health conditions

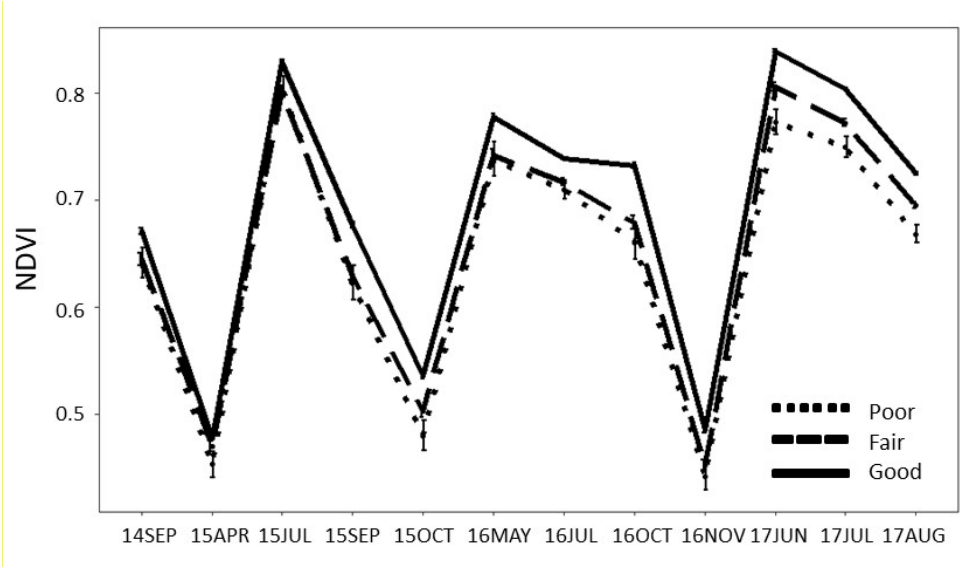

Figure s2 Median NDVI1 values for each of three health conditions from 2014 to 2017 during leaf-on period.

Table s1 Image information of 12 WV-3 images

Time	Season	Day of Year
28-Sep-14	Early leaf senescence	271
18-Apr-15	Early leaf emergence	108
16-Jul-15	Full leaf expansion	197
17-Sep-15	Early leaf senescence	260
31-Oct-15	Late leaf senescence	304
16-May-16	Late leaf emergence	137
24-Jul-16	Full leaf expansion	206
11-Oct-16	Late leaf senescence	285
18-Nov-16	Late leaf senescence	323
11-Jun-17	Full leaf expansion	162
30-Jul-17	Full leaf expansion	211
30-Aug-17	Full leaf expansion	242

Table s2. ANOVA test for pseudo-invariant objects

Month	Average	Lower CI 95%	Upper CI 95%
June	0.126	0.111	0.140
July	0.125	0.111	0.140
August	0.130	0.116	0.144

Note: The ANOVA test finding no significant difference in mean NDVI among image dates had a *P* value of 0.88. The residuals were normally distributed, and the variances are equal (Brown-Forsythe test, P=0.981)

Table s3 ANOVA test for two types of background

Background Type	Average	Lower CI 95%	Upper CI 95%
Mixed	0.728	0.714	0.741
None-vegetated	0.710	0.687	0.733

Note: The ANOVA test finding no significant difference in mean NDVI among image dates had a *P* value of 0.2. The residuals were normally distributed, and the variances are equal (Brown-Forsythe test, P=0.384)

Table s4 Number of trees within the three health condition classes for the top five species.

	Poor	Fair	Good	Sum
American elm	1	26	175	202
Red oak	3	18	121	142
Pin oak	9	25	95	129
Red maple	10	86	164	260
Willow oak	6	65	376	447

Table s5 Chi-square values from non-parametric Wilcoxon/Kruskal-Wallis separating VI means among trees in good, fair and poor condition classes for American elm. For this and subsequent tables, the bold value denotes the most sensitive image date/VI combination. Statistically significant ($p < 0.05$) tests are in red.

Vegetation Index	June		July		August	
	Chi-square	P>ChiSq	Chi-square	P>ChiSq	Chi-square	P>ChiSq
NDVI1	4.44	0.11	0.4882	0.7834	3.1973	0.2022
NDVI2	4.0684	0.1308	0.4141	0.813	2.9087	0.2336
RENDVI1	5.6096	0.0605	2.4034	0.3007	1.7963	0.4073
RENDVI2	3.6469	0.1615	2.2661	0.3221	0.7242	0.6962
Green Yellow ratio	5.10	0.078	1.9044	0.3859	2.438	0.2955
Green Red ratio	6.6127	0.0366	0.4615	0.7939	3.2143	0.2005

Table s6 Chi-square values from non-parametric Wilcoxon/Kruskal-Wallis separating VI means among trees in good, fair and poor condition classes for red oak.

Vegetation Index	June		July		August	
	Chi-square	P>ChiSq	Chi-square	P>ChiSq	Chi-square	P>ChiSq
NDVI1	5.2389	0.0728	7.8841	0.0194	9.1013	0.0106
NDVI2	4.4924	0.1058	8.2025	0.0166	6.0391	0.0488
RENDVI1	7.1241	0.0284	5.7159	0.0574	4.8124	0.0902
RENDVI2	3.7627	0.1524	4.633	0.0986	3.6675	0.1598
Green Yellow ratio	6.1451	0.0463	9.4742	0.0088	7.5254	0.0232
Green Red ratio	6.1538	0.0461	9.8965	0.0071	5.574	0.0616

Table s7 Chi-square values from non-parametric Wilcoxon/Kruskal-Wallis separating VI means among trees in good, fair and poor health condition classes for red maple.

Vegetation Index	June		July		August	
	Chi-square	P>ChiSq	Chi-square	P>ChiSq	Chi-square	P>ChiSq

NDVI1	29.9469	<0.0001	31.3282	<0.0001	16.5029	0.0003
NDVI2	32.7131	<0.0001	32.0169	<0.0001	19.4022	<0.0001
RENDVI1	24.7394	<0.0001	30.424	<0.0001	6.2454	0.044
RENDVI2	30.4282	<0.0001	33.919	<0.0001	6.8311	0.0329
Green Yellow ratio	8.1561	0.0169	11.4977	0.0032	4.2895	0.1171
Green Red ratio	24.9307	<0.0001	11.3198	0.0035	4.0845	0.1297

Table s8 Chi-square values from non-parametric Wilcoxon/Kruskal-Wallis separating VI means among trees in good, fair and poor health condition classes for pin oak.

Vegetation Index	June		July		August	
	Chi-square	P>ChiSq	Chi-square	P>ChiSq	Chi-square	P>ChiSq
NDVI1	23.279	<0.0001	25.2396	<0.0001	16.7129	0.0002
NDVI2	23.6311	<0.0001	23.9345	<0.0001	17.098	0.0002
RENDVI1	10.3354	0.0057	6.9747	0.0306	0.2662	0.8754
RENDVI2	9.5863	0.0083	5.8788	0.0529	1.1273	0.5691
Green Yellow ratio	17.1886	0.0002	16.1929	0.0003	9.5148	0.0086
Green Red ratio	16.4918	0.0003	18.2798	0.0001	11.9735	0.0025

Table s9 Chi-square values from non-parametric Wilcoxon/Kruskal-Wallis separating VI means among trees in good, fair and poor health condition classes for Willow oak.

Vegetation Index	June		July		August	
	Chi-square	P>ChiSq	Chi-square	P>ChiSq	Chi-square	P>ChiSq
NDVI1	7.7428	0.0208	8.0214	0.0181	6.9741	0.0306
NDVI2	6.6044	0.0368	6.5345	0.0381	6.2732	0.0434
RENDVI1	15.949	0.0003	19.0574	<0.0001	12.4481	0.002
RENDVI2	17.195	0.0002	15.1112	0.0005	13.1384	0.0014
Green Yellow ratio	3.7075	0.1566	3.1059	0.2116	5.4296	0.0662
Green Red ratio	1.5415	0.4627	2.5702	0.2766	0.087	0.9574

Table s10 Confusion matrix for discriminating tree health conditions using Random Forest

	Reference		
	Good	**Fair**	**Poor**
Good	95	463	16
Fair	2	1	0
Poor	0	0	0

Graphical Abstract

Three field-measured health classes of 2308 street trees in central Washington D.C. have statistically different WorldView-3 vegetation index values on each of three image dates during 2017 growing season.